

Cross-scale interaction of host tree size and climatic water deficit governs bark beetle-induced tree mortality

Michael J. Koontz^{1,2,3*}, Andrew M. Latimer^{1,2}, Leif A. Mortenson⁴, Christopher J. Fettig⁵, Malcolm P. North^{1,2,6}

¹Graduate Group in Ecology, University of California, Davis, CA, USA

²Department of Plant Sciences, University of California, Davis, CA, USA

³Earth Lab, University of Colorado-Boulder; Boulder, CO, USA

⁴USDA Forest Service, Pacific Southwest Research Station, Placerville, CA, USA

⁵USDA Forest Service, Pacific Southwest Research Station, Davis, CA, USA

⁶USDA Forest Service, Pacific Southwest Research Station, Mammoth Lakes, CA, USA

*Correspondence: michael.koontz@colorado.edu

Keywords: *Dendroctonus brevicomis*, disturbance, drones, *Pinus ponderosa*, Sierra Nevada, structure from motion, forest structure, climate change-type drought, macroecology, Gaussian process

Date report generated: December 21, 2020

Abstract

The recent Californian hot drought (2012-2016) precipitated unprecedented ponderosa pine (*Pinus ponderosa*) mortality, largely attributable to the western pine beetle (*Dendroctonus brevicomis*; WPB). Broad-scale climate conditions can directly shape tree mortality patterns, but mortality rates respond non-linearly to climate when local-scale forest characteristics influence the behavior of tree-killing bark beetles (e.g., WPB). To test for these cross-scale interactions, we conduct aerial drone surveys at 32 sites along a gradient of climatic water deficit (CWD) spanning 350 km of latitude and 1000 m of elevation in WPB-impacted Sierra Nevada forests. We map, measure, and classify over 450,000 trees within 9 km², validating measurements with coincident field plots. We find greater size, proportion, and density of ponderosa pine (the WPB host) increase host mortality rates, as does greater CWD. Critically, we find a CWD/host size interaction such that larger trees amplify host mortality rates in hot/dry sites. Management strategies for climate change adaptation should consider how bark beetle disturbances can depend on cross-scale interactions, which challenge our ability to predict and understand patterns of tree mortality.

28 Introduction

29 Bark beetles dealt the final blow to many of the nearly 150 million trees killed in the California hot drought
30 of 2012 to 2016 and its aftermath.¹ A harbinger of climate change effects to come, record high temperatures
31 exacerbated the drought,^{2,3} which increased water stress in trees,^{4,5} making them more susceptible to
32 colonization by bark beetles.^{6,7} Further, a century of fire suppression has enabled forests to grow into dense
33 stands, which can also make them more vulnerable to bark beetles.^{6,8,9} This combination of environmental
34 conditions and forest structural characteristics led to tree mortality events of unprecedented size across the
35 state.^{10,11}

36 Tree mortality exhibited a strong latitudinal and elevational gradient^{4,11} that can only be partially explained
37 by coarse-scale measures of environmental conditions (i.e., historic climatic water deficit; CWD) and current
38 forest structure (i.e., current regional basal area).¹¹ Progressive loss of canopy water content offers additional
39 insight into tree stress and mortality risk, but cannot ultimately resolve which trees are actually killed by
40 bark beetles or elucidate factors driving bark beetle population dynamics and spread.⁵ Bark beetles respond
41 to local forest characteristics in positive feedbacks that non-linearly alter tree mortality dynamics against a
42 background of environmental conditions that stress trees.^{12,13} Thus, an explicit consideration of local forest
43 structure and composition^{14,15} as well as its cross-scale interaction with regional climate conditions¹⁶ can
44 refine our understanding of tree mortality patterns from California's recent hot drought. The challenge of
45 simultaneously measuring the effects of both local-scale forest features (such as structure and composition)
46 and broad-scale environmental conditions (e.g., CWD) on forest insect disturbance leaves their interaction
47 effect relatively underexplored.^{14–17}

48 The ponderosa pine/mixed-conifer forests in California's Sierra Nevada region are characterized by regular bark
49 beetle disturbances, primarily by the influence of western pine beetle (*Dendroctonus brevicomis*; WPB) on its
50 host ponderosa pine (*Pinus ponderosa*).¹⁸ WPB is a primary bark beetle—its reproductive success is contingent
51 upon host tree mortality, which itself requires enough beetles to mass attack the host tree and overwhelm its
52 defenses.¹⁹ This Allee effect creates a strong coupling between beetle selection behavior of host trees and
53 host tree susceptibility to colonization.^{19–21} A key defense mechanism of conifers to bark beetle attack is to
54 flood beetle bore holes with resin, which physically expels colonizing beetles, can be toxic to the colonizers
55 and their fungi, and may interrupt beetle communication.^{22,23} Under normal conditions, weakened trees
56 with compromised defenses are the most susceptible to colonization and will be the main targets of primary
57 bark beetles like WPB.^{13,23,24} Under severe water stress however, many trees no longer have the resources
58 available to mount a defense.^{7,13} Drought,^{12,25–27} especially when paired with high temperatures,^{24,28–30} can
59 trigger increased bark beetle-induced tree mortality as average tree vigor declines. As the local population

60 density of beetles increases due to successful reproduction within spatially-aggregated susceptible trees, mass
61 attacks grow in size and become capable of overwhelming formidable tree defenses. Even large healthy trees
62 may be susceptible to colonization and mortality when beetle population density is high.^{13,23,24} Thus, water
63 stress and beetle population density interact to influence whether individual trees are susceptible to bark
64 beetles. When extreme or prolonged drought increases host tree vulnerability, bark beetle population growth
65 rates increase, then become self-amplifying as greater beetle densities make additional host trees prone to
66 successful mass attack.^{12,13,15,24}

67 WPB activity is strongly influenced by forest structure– the spatial arrangement and size distribution of trees–
68 and tree species composition. Taking forest structure alone, high-density forests are more prone to bark
69 beetle-induced tree mortality compared to thinned forests^{6,9} which may arise as greater competition for water
70 resources amongst crowded trees lowers average tree resistance,³¹ or because smaller gaps between trees protect
71 pheromone plumes from dissipation by the wind and thus enhance intraspecific beetle communication.³² Tree
72 size is another aspect of forest structure that affects bark beetle host selection behavior with smaller trees
73 tending to have lower capacity for resisting attack, but larger trees being more desirable targets on account
74 of their thicker phloem providing greater nutritional content.^{13,33–35} Throughout an outbreak, some bark
75 beetle species will collectively “switch” the preferred size of tree to attack in order to navigate this trade-off
76 between host susceptibility and host quality.^{13,21,36–39} Taking forest composition alone, WPB activity in the
77 Sierra Nevada mountain range of California is necessarily tied to the regional distribution of its exclusive host,
78 ponderosa pine.¹⁸ Colonization by primary bark beetles can also depend on the local relative frequencies of
79 tree species in forest stands, reflecting the more general pattern that specialist insect herbivory tends to be
80 lower in taxonomically diverse forests compared to monocultures.^{40,41}

81 The interaction between forest structure and composition at both stand- and tree- scales also drives WPB
82 activity. For instance, dense forest stands with high host availability may experience greater beetle-induced
83 tree mortality because dispersal distances between potential host trees are shorter, which reduces predation
84 of adults searching for hosts and facilitates higher rates of colonization.^{33,42,43} High host availability can also
85 reduce the chance of individual beetles wasting their limited resources flying to and landing on a non-host
86 tree.^{44,45} At a finer scale, a host tree’s defensive capacity can depend on its canopy position, with reduced
87 biochemical defenses in suppressed, crowded trees.⁴⁶ Coarse-scale measures of forest structure and composition
88 can therefore only partially explain mechanisms affecting bark beetle disturbance. Finer-grain information is
89 also needed that explicitly recognizes tree species, size, and local density, which better capture the ecological
90 processes underlying insect-induced tree mortality.^{28,36,38,39}

91 The vast spatial extent of WPB-induced tree mortality in the 2012 to 2016 California hot drought challenges

92 our ability to simultaneously consider how broad-scale environmental conditions may interact with local
93 forest structure and composition to affect the dynamic between bark beetle selection and colonization of host
94 trees, and host tree susceptibility to attack.^{15,47} Measuring local forest structure generally requires expensive
95 instrumentation^{4,48} or labor-intensive field surveys,^{14,15,49} which constrains survey extent and frequency.
96 Small, unhumanned aerial systems (sUAS) enable relatively fast and cheap remote imaging over hundreds of
97 hectares of forest, which can be used to measure complex forest structure and composition at the individual
98 tree scale with Structure from Motion (SfM) photogrammetry.^{50,51} The ultra-high, centimeter-scale resolution
99 of sUAS-derived measurements as well as the ability to incorporate vegetation reflectance can help overcome
100 challenges in species classification and dead tree detection inherent in other remote sensing methods, such
101 as airborne LiDAR.⁵² Distributing such surveys across an environmental gradient can overcome the data
102 acquisition challenge inherent in investigating phenomena with both a strong local- and a strong broad-scale
103 component.

104 We used sUAS-derived remote sensing images over a network of 32 sites in Sierra Nevada ponderosa pine/mixed-
105 conifer forests spanning 1000 m of elevation and 350 km of latitude¹⁴ covering a total of 9 km², to investigate
106 how broad-scale environmental conditions interacted with local forest structure and composition to shape
107 patterns of tree mortality during the cumulative tree mortality event of 2012 to 2018. We asked:

- 108 1. How does the proportion of the ponderosa pine host trees in a local area and average host tree size
109 affect WPB-induced tree mortality?
- 110 2. How does the density of all trees (hereafter “overall density”) affect WPB-induced tree mortality?
- 111 3. How does the total basal area of all trees (hereafter “overall basal area”) affect WPB-induced tree
112 mortality?
- 113 4. How does environmentally-driven tree moisture stress affect WPB-induced tree mortality?
- 114 5. How do the effects of forest structure, forest composition, and environmental condition interact to
115 influence WPB-induced tree mortality?

116 Here, we show that a greater local proportion of host trees (ponderosa pine) strongly increases the probability
117 of host mortality, with greater host density amplifying this effect. We also show that greater site-level
118 CWD increases host mortality rates. Further, we show that larger host trees increase the probability of host
119 mortality in accordance with well-known life history of WPB. Critically, we find a strong interaction between
120 host size and CWD such that host mortality rates are especially high in hot/dry sites where the local average
121 host tree size is large. Our results demonstrate a cross-scale interaction in the response of WPB to local

122 forest structure and composition across an environmental gradient, which helps reconcile differences between
 123 observed ecosystem-wide tree mortality patterns and predictions from models based on coarser-scale forest
 124 structure.

125 Results

126 Tree detection algorithm performance

127 We found that the experimental `lmfx` algorithm⁵³ with parameter values of `dist2d = 1` and `ws = 2.5`
 128 performed the best across 7 measures of forest structure as measured by Pearson’s correlation with ground
 129 data (Table 1).

Table 1: Correlation and differences between the best performing tree detection algorithm (`lmfx` with `dist2d = 1` and `ws = 2.5`) and the ground data. An asterisk next to the correlation or RMSE indicates that this value was within 5% of the value of the best-performing algorithm/parameter set. Ground mean represents the mean value of the forest metric across the 110 field plots that were visible from the sUAS-derived imagery. The median error is calculated as the median of the differences between the air and ground values for the 110 visible plots. Thus, a positive number indicates an overestimate by the sUAS workflow and a negative number indicates an underestimate.

Forest structure metric	Ground mean	Correlation with ground	RMSE	Median error
total tree count	19	0.67*	8.68*	2
count of trees > 15 m	9.9	0.43	7.38	0
distance to 1st neighbor (m)	2.8	0.55*	1.16*	0.26
distance to 2nd neighbor (m)	4.3	0.61*	1.70*	0.12
height (m); 25 th percentile	12	0.16	8.46	-1.2
height (m); mean	18	0.29	7.81*	-2.3
height (m); 75 th percentile	25	0.35	10.33*	-4

130 Classification accuracy for live/dead and host/non-host

131 The accuracy of live/dead classification on a withheld testing data set was 96.4%. The accuracy of species
 132 classification on a withheld testing dataset was 64.1%. The accuracy of WPB host/non-WPB-host (i.e.,
 133 ponderosa pine versus other tree species) on a withheld testing dataset was 71.8%.

134 Site summary based on best tree detection algorithm and classification

135 Across all study sites, we detected, segmented, and classified 452,413 trees in 23,187, 20 x 20m pixels (with
 136 the area of each pixel being approximately equivalent to that of a field plot). Of these trees, we classified

137 118,879 as dead (26.3% mortality). Estimated site-level tree mortality ranged from 6.8% to 53.6%. See
 138 Supplementary Table 1 for site summaries and comparisons to site-level mortality measured from field data.

139 **Effect of local structure and regional climate on tree mortality attributed to WPB**

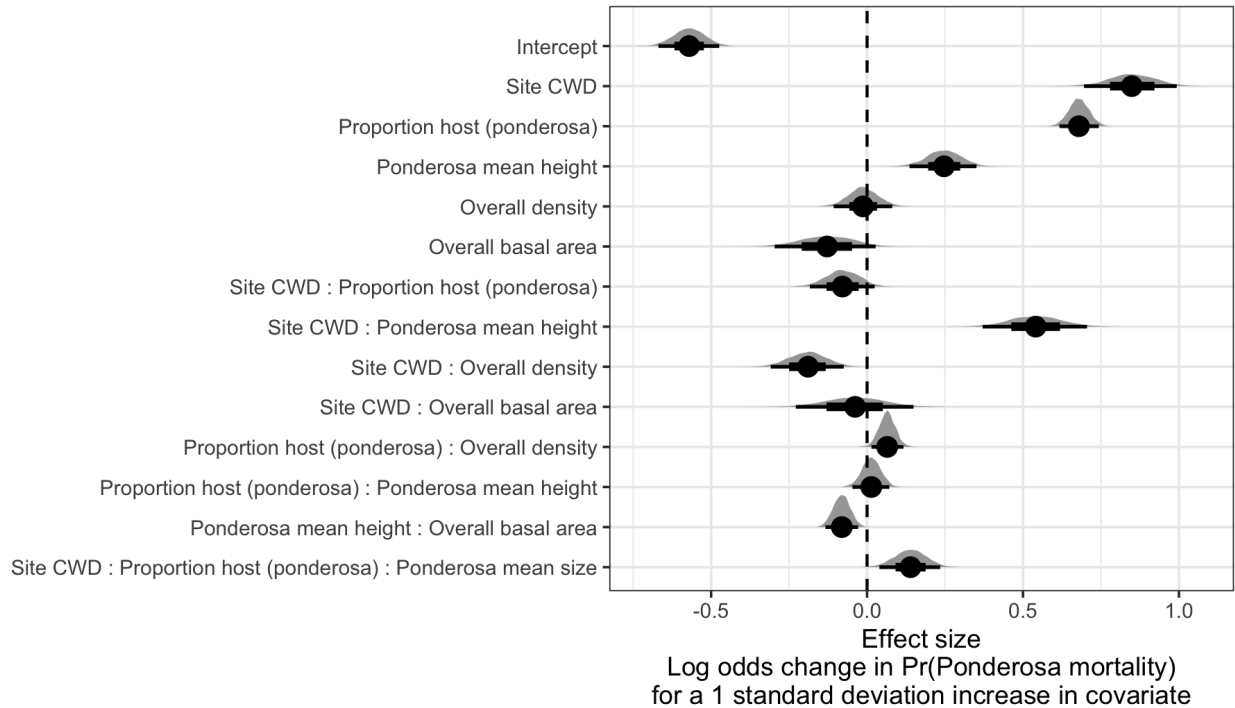


Figure 1: Posterior distributions of effect size from zero-inflated binomial model predicting the probability of ponderosa pine mortality in a 20 x 20-m cell given forest structure characteristics and site-level climatic water deficit (CWD). The gray filled area for each model covariate represents the probability density of the posterior distribution, the point underneath each density curve represents the median of the estimate, the bold interval surrounding the point estimate represents the 66% credible interval, and the thin interval surrounding the point estimate represents the 95% credible interval. Estimates for all model parameters, including Gaussian Process parameters for each site, can be found in Supplementary Table 2.

140 Site-level CWD exerted a positive main effect on the probability of ponderosa mortality (effect size: 0.85;
 141 95% CI: [0.70, 0.99]; Figure 1). We found a positive main effect of proportion of host trees per cell (effect size:
 142 0.68; 95% CI: [0.62, 0.74]), with a greater proportion of host trees (i.e., ponderosa pine) in a cell increasing
 143 the probability of ponderosa pine mortality. We detected no effect of overall tree density or overall basal area
 144 (i.e., including both ponderosa pine and non-host species; tree density effect size: -0.01; 95% CI: [-0.11, 0.08];
 145 basal area effect size: -0.13; 95% CI: [-0.29, 0.03]).

146 We found a positive two-way interaction between the overall tree density per cell and the proportion of trees
 147 that were hosts, which is equivalent to a positive effect of the density of host trees (effect size: 0.06; 95% CI:
 148 [0.01, 0.12]; Figure 1).

149 We found a positive main effect of mean height of ponderosa pine on the probability of ponderosa mortality
150 (effect size: 0.25; 95% CI: [0.14, 0.35]). Coupled with the strong correlation between proportion of dead host
151 trees and basal area killed (See Supplementary Figure 1 and Supplementary Note 1), these results suggest
152 that WPB attacked larger trees, on average. Further, there was a strong positive interaction between CWD
153 and ponderosa pine mean height, such that larger trees were especially likely to increase the local probability
154 of ponderosa mortality in hotter, drier sites (effect size: 0.54; 95% CI: [0.37, 0.70]; Figure 2).

155 We found no effect of the site-level CWD interactions with the proportion of host trees (effect size: -0.08;
156 95% CI: [-0.18, 0.03]) or of the interaction between CWD and total basal area (effect size: -0.04; 95% CI:
157 [-0.23, 0.15]; Figure 1).

158 We found a negative effect of the CWD interaction with overall tree density (effect size: -0.19; 95% CI: [-0.31,
159 -0.07]) as well as of the interaction between mean height of host trees and the overall basal area (effect size:
160 -0.08; 95% CI: [-0.13, -0.03]; Figure 1).

161 While we found no interaction between proportion of host trees and mean host tree height, we did find a
162 3-way interaction between these variables with CWD (effect size: 0.14; 95% CI: [0.04, 0.24]; Figure 1).

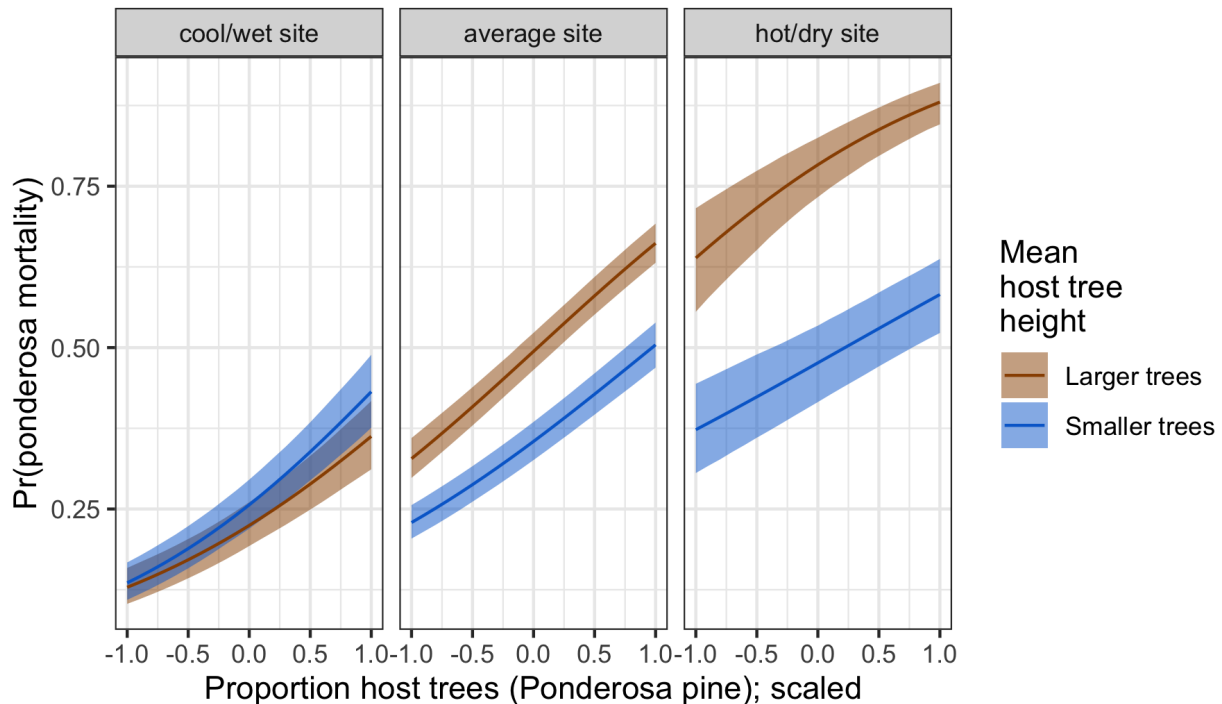


Figure 2: Line version of model results with 95% credible intervals showing primary influence of ponderosa pine structure on the probability of ponderosa pine mortality, and the interaction across climatic water deficit. The ‘larger trees’ line represents the mean height of ponderosa pine 0.7 standard deviations above the mean (approximately 24.1 m), and the ‘smaller trees’ line represents the mean height of ponderosa pine 0.7 standard deviations below the mean (approximately 12.1 m).

163 Discussion

164 This study uses drone-derived imagery to refine our understanding of the patterns of tree mortality following
165 the 2012 to 2016 California hot drought and its aftermath. By simultaneously measuring the effects of
166 local forest structure and composition across broad-scale environmental gradients, we were able to better
167 characterize the influence of a tree-killing insect, the WPB, compared to using correlates of tree stress alone.

168 Strong positive main effect of CWD

169 We found a strong positive effect of site-level CWD on ponderosa pine mortality rate. We did not measure
170 tree water stress at an individual tree level as in other recent work,¹⁵ and instead treated CWD as a general
171 indicator of tree stress following results of coarser-scale studies.¹¹ When measured at a fine scale, even if not
172 at an individual tree level, progressive canopy water loss can be a good indicator of tree water stress and
173 increased vulnerability to mortality from drought or bark beetles.⁵ Though our entire study area experienced
174 exceptional hot drought between 2012 and 2016,^{2,3} using a 30-year historic average of CWD as a site-level
175 indicator of tree stress doesn't allow us to disentangle whether water availability was lower in an absolute
176 sense during the drought or whether increasing tree vulnerability to bark beetles was driven by chronic water
177 stress at these historically hotter/drier sites.⁵⁴

178 Positive effect of host proportion and density

179 A number of mechanisms associated with the relative abundance of species in a local area might underlie the
180 strong effect of host proportion on the probability of host tree mortality. Frequency-dependent herbivory—
181 whereby mixed-species forests experience less herbivory compared to monocultures (as an extreme example)—
182 is common, especially for oligophagous insect species.⁴⁰ Non-host volatiles reduce attraction of several species
183 of bark beetles to their aggregation pheromones,⁵⁵ including WPB.⁵⁶ Combinations of non-host volatiles and
184 an antiaggregation pheromone have been used successfully to reduce levels of tree mortality attributed to
185 WPB in California.^{57,58} The positive relationship between host density and susceptibility to colonization by
186 bark beetles has been so well-documented at the experimental plot level^{43,59,60} that lowering stand densities
187 through selective harvest of hosts is commonly recommended for reducing future levels of tree mortality
188 attributed to bark beetles,⁶¹ including WPB.¹⁸ Greater host density shortens the flight distance required
189 for WPB to disperse to new hosts, which likely facilitates bark beetle spread, however we calibrated our
190 aerial tree detection to ~400 m² areas rather than to individual tree locations, so our data are insufficient to
191 address these relationships. Increased density of ponderosa pine, specifically, may disproportionately increase
192 the competitive environment for host trees (and thus increase their susceptibility to WPB colonization) if

193 intraspecific competition amongst ponderosa pine trees is stronger than interspecific competition as would
194 be predicted with coexistence theory.⁶² Finally, greater host densities increase the frequency that searching
195 WPB land on hosts, rather than non-hosts, thus reducing the amount of energy expended during host finding
196 and selection as well as the time that searching WPB spend exposed to a variety of predators outside the
197 host tree.

198 **No main effect of overall density, but interaction with CWD**

199 We detected no relationship between overall tree density and ponderosa pine mortality, though work from the
200 coincident ground plots showed a negative but weak relationship when using proportion of trees killed as a
201 response.¹⁴ Kaiser et al. ²⁸ also show greater mountain pine beetle (*Dendroctonus ponderosae*) infestation in
202 lower-density sites in Montana. However, Hayes et al. ³¹ and Fettig et al. ¹⁴ found that measures of overall
203 tree density explained more variation in tree mortality than measures of host availability, though those
204 conclusions were based on broader-scale analyses³¹ or a different response variable (i.e., “total number of
205 dead host trees”¹⁴ rather than a binomial response of “number of dead host trees conditional on the total
206 number of host trees” as in our study).

207 Our greater sample size may have enabled us to more finely parse the role of multi-faceted forest structure
208 and composition, along with CWD and interactions, in driving ponderosa pine mortality rates. Indeed, we
209 did find a negative two-way interaction between site CWD and overall density, suggesting denser stands
210 experienced lower rates of ponderosa mortality in hotter, drier sites, which comports with Restaino et al. ⁹ in
211 results from their unmanipulated gradient of overall density in the same region during the same hot drought.
212 In the absence of active management, forest structure is largely a product of climate and, with increasing
213 importance at finer spatial scales, topographic conditions.⁶³ Denser forest patches in our study may indicate
214 greater local water availability, more favorable conditions for tree growth and survivorship, and increased
215 resistance to beetle-induced tree mortality, especially when denser patches are found in hot, dry sites.^{9,63,64}

216 **Effect of overall basal area**

217 While overall tree density is likely an indicator of favorable microsites in fire-suppressed forests, overall basal
218 area is a better indicator of the local competitive environment especially in water-limited forests.^{63,64} However,
219 we found no main effect of overall basal area on the probability of ponderosa mortality, nor of its interaction
220 with site-level CWD. This contrasts to the results from Young et al. ¹¹, and from analyses of coincident
221 field plots.¹⁴ While the contrast to Young et al. ¹¹ might be explained by different scales of analyses (i.e.,
222 3500 x 3500 m pixels vs. 20 x 20 m pixels), the contrast with the coincident ground plots is more puzzling.

223 One explanation is that the drone sampling captured more area beyond the conditionally-sampled field plots
224 (i.e., 10% ponderosa pine basal area mortality was a criterion for plot selection) that reflected a different
225 relationship between local basal area and tree mortality. Perhaps more likely is that our measure of total basal
226 area isn't precise enough to represent the local competitive environment compared to field-derived basal area.
227 For our study, basal area was derived from species-specific and inherently noisy allometric relationships with
228 tree height, which itself was derived from the SfM processing of drone imagery. As remote sensing technology
229 improves to enable finer-scale information extraction (e.g., individual tree measurements), more dialogue
230 between ecologists of all stripes⁶⁵⁻⁶⁷ is needed to fully imagine how to best measure natural phenomena
231 remotely, either by adopting wheels already invented (e.g., plot basal area) or by innovating something brand
232 new.

233 **Positive main effect of host tree mean size**

234 The positive main effect of host tree mean size on ponderosa mortality rates tracks the conventional wisdom
235 on the dynamics of WPB in the Sierra Nevada, as well as other primary bark beetles.¹⁸ WPB exhibit a
236 preference for trees 50.8 to 76.2 cm DBH,^{68,69} and a positive relationship between host tree size and levels of
237 tree mortality attributed to WPB was reported by Fettig et al.¹⁴ in the coincident field plots as well as in
238 other recent studies.^{9,15,70} Larger trees are more nutritious and are therefore ideal targets if local bark beetle
239 density is high enough to successfully initiate mass attack and overwhelm tree defenses, as can occur when
240 many trees are under water stress.^{7,13,24} In the recent hot drought, we expected that most trees would be
241 under severe water stress, setting the stage for increasing beetle density, successful mass attacks, and targeting
242 of larger trees. Given that our dead tree height calibration was conservative (accounting for underestimates
243 of drone-derived dead tree heights relative to field-measured trees), it is likely that the positive main effect of
244 tree height that we report represents a lower bounds of this effect. Additionally, Fettig et al.¹⁴ found no tree
245 size/mortality relationship for incense cedar or white fir in the coincident field plots. These species represent
246 22.3% of the total tree mortality observed in their study, yet in our study all dead trees were classified as
247 ponderosa pine (see Methods) which could have further dampened the positive effect of tree size on tree
248 mortality that we identified.

249 **Cross-scale interaction of CWD and host tree size**

250 In hotter, drier sites, a larger average host size increased the probability of host mortality. Notably, a
251 similar pattern was shown by Stovall et al.⁶⁵ in a study confined to the southern Sierra Nevada (i.e., the
252 hottest, driest portion of the more spatially extensive results we present here) with a strong positive tree
253 height/mortality relationship in areas with the greatest vapor pressure deficit and no tree height/mortality

254 relationship in areas with the lowest vapor pressure deficit. Our work suggests that the WPB was cueing
255 into different aspects of forest structure across an environmental gradient in a spatial context in a parallel
256 manner to the temporal context noted by Stovall et al. ⁶⁵ and Pile et al. ⁷⁰, who observed that mortality was
257 increasingly driven by larger trees as the hot drought proceeded and became more severe. A temporal signal of
258 bark beetles attacking larger and larger host trees reflects the positive feedback between forest structure and
259 bark beetle population dynamics as the population phase cycles from endemic to epidemic.¹³ This positive
260 feedback leading to eruptive population dynamics is well-documented as a temporal phenomenon, and here
261 we show a similar pattern in a spatial context mediated through site-level CWD.

262 A key difference from the endemic-to-epidemic positive feedback noted by Boone et al. ¹³ is that none of our
263 study areas were considered to be in an endemic population phase by typical measures of WPB dynamics.^{31,33}
264 WPB dynamics at all sites were considered epidemic, with >5 trees killed per ha (see Supplementary Table 1).
265 The cross-scale interaction between broad-scale CWD and local-scale host tree size, even amongst populations
266 all in an epidemic phase, highlights the dramatic implications of the positive feedback for landscape-scale tree
267 mortality. The massive tree mortality in hotter/drier Sierra Nevada forests (lower latitudes and elevations^{4,11})
268 during the 2012 to 2016 hot drought likely arose as a synergistic alignment of environmental conditions and
269 local forest structure that allowed WPB to successfully colonize large trees, rapidly increase in population
270 size, and expand. The unexpectedly low mortality in cooler/wetter Sierra Nevada forests compared to model
271 predictions based on coarser-scale forest structure data¹¹ may result from a different WPB response to
272 local forest structure due to a lack of an alignment with favorable climate conditions and a weaker positive
273 feedback.

274 **Limitations and future directions**

275 We have demonstrated that drones can be effective means of collecting forest data at multiple, vastly different
276 spatial scales to investigate a single, multi-scale phenomenon— from meters in between trees, to hundreds of
277 meters of elevation, to hundreds of thousands of meters of latitude. Some limitations remain, but can be
278 overcome with further refinements in the use of this tool for forest ecology. Most of these limitations arise
279 from classification and measurement of standing dead trees, making it imperative to work with field data for
280 calibration and uncertainty reporting.

281 The greatest limitation in our study arising from classification uncertainty is in the assumption that all dead
282 trees were ponderosa pine, which we estimate from coincident field plots is true approximately 73.4% of the
283 time. Because the forest structure factors influencing the likelihood of individual tree mortality during the hot
284 drought depended on tree species,¹⁵ we cannot rule out that some of the ponderosa pine mortality relationships

285 to forest structure that we observed may be partially explained by those relationships in other species that
286 were misclassified as ponderosa pine using our methods. However, the overall community composition across
287 our study area was similar¹⁴ and we are able to reproduce similar forest structure/mortality patterns in
288 drone-derived data when restricting the scope of analysis to only trees detected in the footprints of the
289 coincident field plots (see Supplementary Figure 2). Thus, we remain confident that the patterns we observed
290 were driven primarily by the dynamic between WPB and ponderosa pine. While spectral information of
291 foliage could help classify living trees to species, the species of standing dead trees were not spectrally distinct.
292 This challenge of classifying standing dead trees to species implies that a conifer forest systems with less
293 bark beetle and tree host diversity, such as mountain pine beetle outbreaks in relative monocultures of
294 naturally-occurring lodgepole pine forests in the Intermountain West, should be particularly amenable to the
295 methods presented here even with minimal further refinement because dead trees will almost certainly belong
296 to a single species and have succumbed to colonization by a single bark beetle species. For similar reasons,
297 these methods would also work particularly well if imagery were also captured prior to the mortality event.

298 Some uncertainty surrounded our ability to detect trees using the geometry of the dense point clouds derived
299 with SfM. The horizontal accuracy (i.e., longitude/latitude position) of the tree detection was better than the
300 vertical accuracy (i.e., height), which may result from a more significant error contribution by the field-based
301 calculations of tree height compared to tree position relative to plot center (Table 1). Height measurements
302 were particularly challenging for standing dead trees, because SfM can fail to produce any points representing
303 narrow, needleless treetops in the resulting dense point cloud. Our conservative calibration of drone-measured
304 tree heights to field-measured heights strengthened the main effect of CWD on host mortality in our model
305 and reversed the effect of host tree height. We report that larger host trees increase the probability of host tree
306 mortality, while models using uncalibrated tree heights show that larger trees decrease host mortality rates (see
307 Supplementary Figure 3 compared to Figure 1). While our live/dead classification was fairly accurate (96.4%
308 on a withheld dataset), our species classifier would likely benefit from better crown segmentation because the
309 pixel-level reflectance values within each crown are averaged to characterize the “spectral signature” of each
310 tree. With better delineation of each tree crown, the mean value of pixels within each tree crown will likely
311 be more representative of that tree’s spectral signature.

312 Better tree detection, crown segmentation, and dead tree height measurement would likely improve with
313 better SfM point clouds which can be enhanced with greater overlap between images⁷¹ or with oblique (i.e.,
314 off-nadir) imagery.⁷² Frey et al. ⁷¹ found that 95% overlap was preferable for generating dense point clouds in
315 forested areas, and James and Robson⁷² reduced dense point cloud errors using imagery taken at 30 degrees
316 off-nadir. We only achieved 91.6% overlap with the X3 RGB camera and 83.9% overlap with the multispectral

317 camera, and all imagery was nadir-facing. We anticipate that computer vision and deep learning will also
318 prove helpful in overcoming some of these detection and classification challenges.⁷³

319 Finally, we note our study is constrained by the uncertainty in measuring basal area from SfM processing of
320 drone-derived imagery. This uncertainty makes it challenging to represent typical field-based measures of
321 local competitive environment (e.g., total plot basal area) or ecosystem impact (e.g., proportion of dead basal
322 area in a plot) in a statistical analysis. Instead, we opted to use the probability of ponderosa mortality as
323 our key response variable, which is well-suited to understanding the dynamics between WPB colonization
324 behavior and host tree susceptibility.

325 **Conclusions**

326 Climate change adaptation strategies emphasize management action that considers whole-ecosystem responses
327 to inevitable change,⁷⁴ which requires a macroecological understanding of how phenomena at multiple
328 scales can interact. Tree vulnerability to environmental stressors presents only a partial explanation for
329 tree mortality patterns during hot droughts, especially when bark beetles are present. We've shown that
330 drones can be a valuable tool for investigating multi-scalar phenomena, such as how local forest structure
331 combines with environmental conditions to shape forest insect disturbance. Understanding the conditions
332 that drive dry western U.S. forest responses to disturbances such as bark beetle outbreaks will be vital for
333 predicting outcomes from increasing disturbance frequency and intensity exacerbated by climate change.⁷⁵
334 Our study suggests that outcomes will depend on interactions between local forest structure and broad-scale
335 environmental gradients, with the potential for cross-scale interactions to enhance our understanding of forest
336 insect dynamics.

337 **Methods**

338 **Study system**

339 We designed the aerial survey to coincide with 160 vegetation/forest insect monitoring plots at 32 sites
340 established between 2016 and 2017 by Fettig et al.¹⁴ (Figure 3). The study sites were chosen to reflect
341 typical west-side Sierra Nevada yellow pine/mixed-conifer forests and were dominated by ponderosa pine.¹⁴
342 Sites were placed in WPB-attacked, yellow pine/mixed-conifer forests across the Eldorado, Stanislaus, Sierra
343 and Sequoia National Forests and were stratified by elevation (914-1219 m, 1219-1524 m, 1524-1829 m above
344 sea level). In the Sequoia National Forest, the southernmost National Forest in our study, sites were stratified
345 with the lowest elevation band of 1219-1524 m and extended to an upper elevation band of 1829-2134 m to
346 capture a more similar forest community composition as at the more northern National Forests. The sites

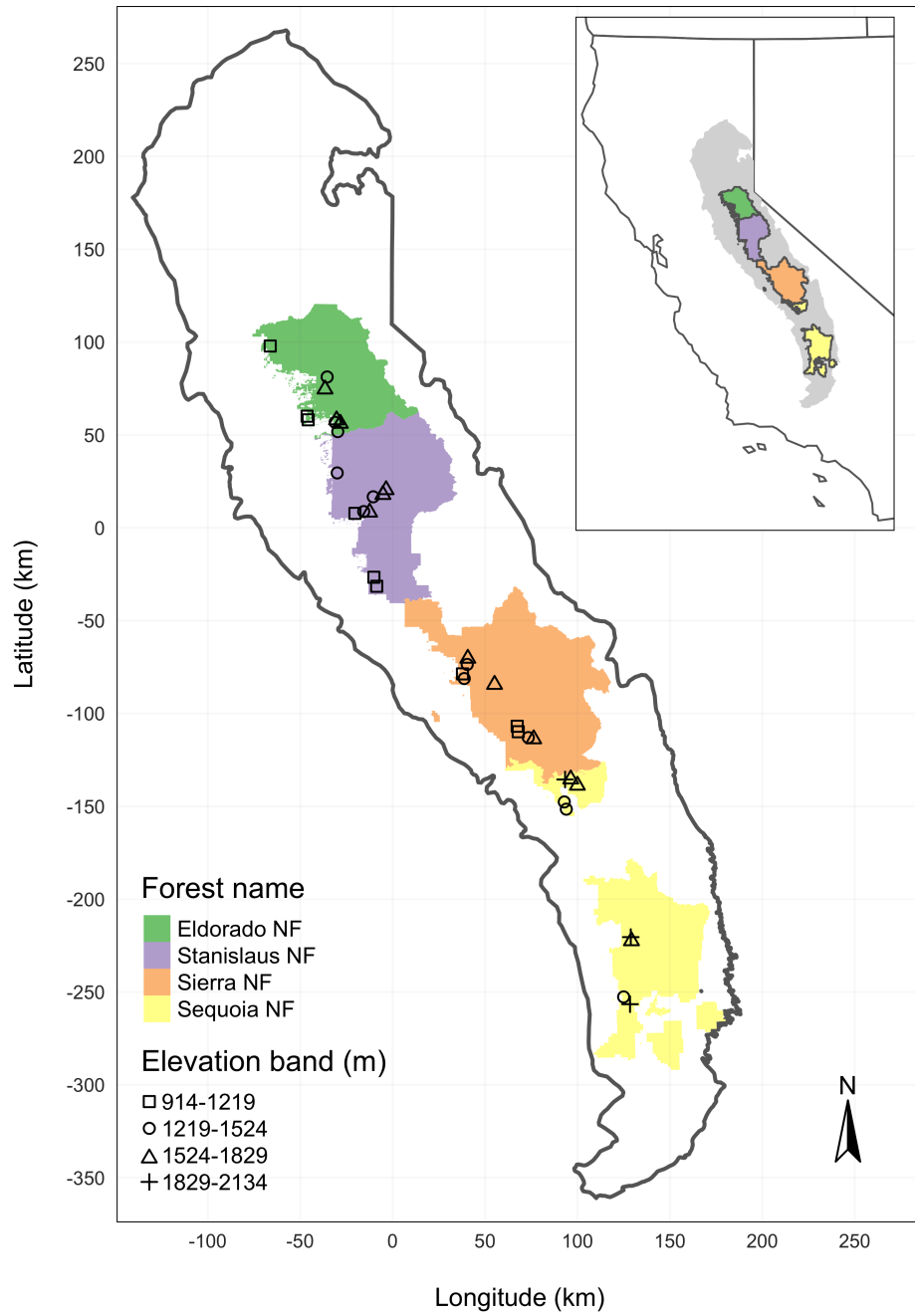


Figure 3: The network of field plots spanned a 350-km latitudinal gradient from the Eldorado National Forest in the north to the Sequoia National Forest in the south. Plots were stratified by three elevation bands in each forest, with the plots in the Sequoia National Forest (the southern-most National Forest) occupying elevation bands 305 m above the three bands in the other National Forests in order to capture a similar community composition.

347 have variable forest structure and plot locations were selected in areas with >35% ponderosa pine basal area
348 and >10% ponderosa pine mortality. At each site, five 0.041-ha circular plots were installed along transects
349 with 80 to 200m between plots. In the field, Fettig et al.¹⁴ mapped all stem locations relative to the center
350 of each plot using azimuth/distance measurements. Tree identity to species, tree height, and diameter at
351 breast height (DBH) were recorded if DBH was greater than 6.35cm. Year of mortality was estimated based
352 on needle color and retention if it occurred prior to plot establishment, and was directly observed thereafter
353 during annual site visits. A small section of bark (approximately 625 cm²) on both north and south aspects
354 was removed from dead trees to determine if bark beetle galleries were present. The shape, distribution, and
355 orientation of galleries are commonly used to distinguish among bark beetle species.¹⁸ In some cases, deceased
356 bark beetles were present beneath the bark to supplement identifications based on gallery formation. During
357 the spring and early summer of 2018, all field plots were revisited to assess whether dead trees had fallen.¹⁴
358 In the typical life cycle of WPBs, females initiate host colonization by tunneling through the outer bark and
359 into the phloem and outer xylem where they rupture resin canals. As a result, oleoresin exudes and collects on
360 the bark surface, as is commonly observed with other bark beetle species. During the early stages of attack,
361 females release an aggregation pheromone component which, in combination with host monoterpenes released
362 from pitch tubes, is attractive to conspecifics.⁷⁶ An antiaggregation pheromone component is produced during
363 latter stages of host colonization by several pathways, and is thought to reduce intraspecific competition
364 by altering adult behavior to minimize overcrowding of developing brood within the host.⁷⁷ Volatiles from
365 several non-hosts sympatric with ponderosa pine have been demonstrated to inhibit attraction of WPB to
366 its aggregation pheromones.^{56,78} In California, WPB generally has 2-3 generations in a single year and can
367 often outcompete other primary bark beetles such as the mountain pine beetle in ponderosa pines, especially
368 in larger trees.³³ WPB population growth rates can, however, be reduced by competition with other beetle
369 species cohabitating in the same host tree, as well as by predation during dispersal to seek a host.³³

370 **Aerial data collection and processing**

371 Nadir-facing imagery was captured using a gimbal-stabilized DJI Zenmuse X3 broad-band red/green/blue
372 (RGB) camera⁷⁹ and a fixed-mounted Micasense Rededge3 multispectral camera with five narrow bands⁸⁰ on
373 a DJI Matrice 100 aircraft.⁸¹ Imagery was captured from both cameras along preprogrammed aerial transects
374 over ~40 ha surrounding each of the 32 sites (each of these containing five field plots) and was processed
375 in a series of steps to yield local forest structure and composition data suitable for our statistical analyses.
376 All images were captured in 2018 during a 3-month period between early April and early July, and thus
377 our work represents a postmortem investigation into the drivers of cumulative tree mortality. Following the

378 call by Wyngaard et al.⁸², we establish “data product levels” to reflect the image processing pipeline from
379 raw imagery (Level 0) to calibrated, fine-scale forest structure and composition information on regular grids
380 (Level 4), with each new data level derived from levels below it. Here, we outline the steps in the processing
381 and calibration pipeline visualized in Figure 4, and include additional details in the Supplementary Methods.

382 **Level 0: Raw data from sensors**

383 Raw data comprised approximately 1900 images per camera lens (one broad-band RGB lens and five narrow-
384 band multispectral lenses) for each of the 32 sites (Figure 4; Level 0; Supplementary Figures 4 and 5). Prior
385 to the aerial survey, two strips of bright orange drop cloth (~100 x 15 cm) were positioned as an “X” over the
386 permanent monuments marking the center of the 5 field plots from Fettig et al.¹⁴ (see Supplementary Figure
387 6).

388 We preprogrammed north-south aerial transects using Map Pilot for DJI on iOS flight software⁸⁴ at an
389 altitude of 120 m above ground level (with “ground” defined using a 1-arc-second digital elevation model⁸⁵).
390 The resulting ground sampling distance was approximately 5 cm/px for the Zenmuse X3 RGB camera and
391 approximately 8 cm/px for the Rededge3 multispectral camera. We used 91.6% image overlap (both forward
392 and side) at the ground for the Zenmuse X3 RGB camera and 83.9% overlap (forward and side) for the
393 Rededge3 multispectral camera.

394 **Level 1: Basic outputs from photogrammetric processing**

395 We used SfM photogrammetry implemented in Pix4Dmapper Cloud (www.pix4d.com) to generate dense
396 point clouds (Figure 4; Level 1, left; Supplementary Figure 7), orthomosaics (Figure 4; Level 1, center;
397 Supplementary Figure 8), and digital surface models (Figure 4; Level 1, right; Supplementary Figure 9)
398 for each field site.⁷¹ For 29 sites, we processed the Rededge3 multispectral imagery alone to generate these
399 products. For three sites, we processed the RGB and the multispectral imagery together to enhance the point
400 density of the dense point cloud. All SfM projects resulted in a single processing “block,” indicating that all
401 images in the project were optimized and processed together. The dense point cloud represents x, y, and z
402 coordinates as well as the color of millions of points per site. The orthomosaic represents a radiometrically
403 uncalibrated, top-down view of the survey site that preserves the relative x-y positions of objects in the scene.
404 The digital surface model is a rasterized version of the dense point cloud that shows the altitude above sea
405 level for each pixel in the scene at the ground sampling distance of the camera that generated the Level 0
406 data.

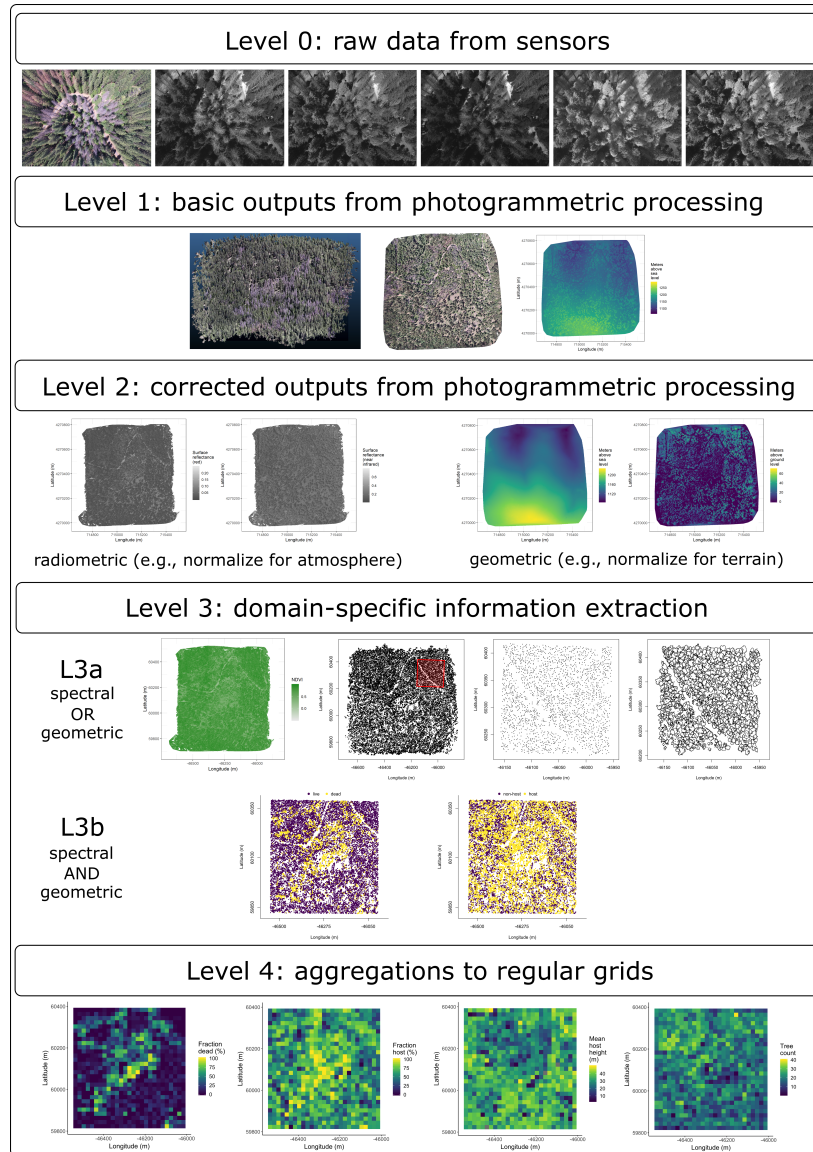


Figure 4: Schematic of the data processing workflow for a single site with each new data product level derived from data at lower levels. Level 0 represents raw data from the sensors. From left to right: RGB photo from DJI Zenmuse X3, output images from Micasense Rededge3 (blue, green, red, near infrared, red edge). Level 1 represents basic outputs from the SfM workflow. From left to right: dense point cloud, RGB orthomosaic, digital surface model (DSM; ground elevation plus vegetation height). Level 2 represents radiometrically or geometrically corrected Level 1 products. From left to right: radiometrically-corrected ‘red’ surface reflectance map, radiometrically-corrected ‘near infrared’ surface reflectance map, digital terrain model (DTM) derived by a geometric correction of the dense point cloud, canopy height model (CHM; DTM subtracted from the DSM). Level 3 represents domain-specific information extraction from Level 2 products and is divided into two sub-levels. Level 3a products are derived using only spectral or only geometric data. From left to right: map of Normalized Difference Vegetation Index (NDVI),⁸³ map of detected trees derived from the CHM, detected trees within red polygon, polygons representing segmented tree crowns within red polygon. Level 3b products are derived using both spectral and geometric data. From left to right: trees classified as alive or dead based on spectral reflectance within each segmented tree crown, trees classified as WPB host/non-host. Level 4 represents aggregations of Level 3 products to regular grids that better reflects the grain size of the validation (e.g., to match area of validation field plots) or which provides neighborhood- rather than individual-scale information (e.g., stand-level proportion of host trees). From left to right: grid representing fraction of dead trees per cell, grid representing fraction of hosts per cell, grid representing mean host height per cell, tree density per cell. All cells measure 20 x 20 m.

407 **Level 2: Corrected outputs from photogrammetric processing**

408 **Radiometric corrections** A radiometrically-corrected reflectance map (Figure 4; Level 2, left two figures;
 409 i.e., a corrected version of the Level 1 orthomosaic; Supplementary Figure 10) was generated using the Pix4D
 410 software by incorporating incoming light conditions for each narrow band of the Rededge3 camera (captured
 411 simultaneously with the Rededge3 camera using an integrated downwelling light sensor) as well as a pre-flight
 412 image of a calibration panel of known reflectance (see Supplementary Table 3 for camera and calibration
 413 panel details).

414 **Geometric corrections** We implemented a geometric correction to the Level 1 dense point cloud and
 415 digital surface model by normalizing these data for the terrain underneath the vegetation. We generated the
 416 digital terrain model representing the ground underneath the vegetation at 1-m resolution (Figure 4; Level
 417 2, third image; Supplementary Figure 11) by classifying each survey area’s dense point cloud into “ground”
 418 and “non-ground” points using a cloth simulation filter algorithm⁸⁶ implemented in the `lidR`⁵³ package and
 419 rasterizing the ground points using the `raster` package.⁸⁷ We generated a canopy height model (Figure 4;
 420 Level 2, fourth image; Supplementary Figure 12) by subtracting the digital terrain model from the digital
 421 surface model.

422 **Level 3: Domain-specific information extraction**

423 **Level 3a: Data derived from spectral or geometric Level 2 product** Using just the spectral
 424 information from the radiometrically-corrected reflectance maps, we calculated several vegetation indices
 425 including the normalized difference vegetation index⁸³ (NDVI; Figure 4; Level 3a, first image; Supplementary
 426 Figure 13), the normalized difference red edge⁸⁸ (NDRE) , the red-green index⁸⁹ (RGI), the red edge
 427 chlorophyll index⁹⁰ ($CI_{red\ edge}$), and the green chlorophyll index⁹⁰ (CI_{green}).

Table 2: Algorithm name, number of parameter sets tested for each algorithm, and references.

Algorithm	Parameter sets tested	Reference(s)
li2012	131	Li et al. ⁹¹ ; Jakubowski et al. ⁹² ; Shin et al. ⁹³
lmfx	30	Roussel ⁹⁴
localMaxima	6	Roussel et al. ⁵³
multichm	1	Eysn et al. ⁹⁵
ptrees	3	Vega et al. ⁹⁶
vwf	3	Plowright ⁹⁷

Algorithm	Parameter sets tested	Reference(s)
watershed	3	Pau et al. ⁹⁸

428 Using just the geometric information from the canopy height model or terrain-normalized dense point cloud,
 429 we generated maps of detected trees (Figure 4; Level 3a, second and third images; Supplementary Figure
 430 14) by testing a total of 7 automatic tree detection algorithms and a total of 177 parameter sets (Table
 431 2). We used the field plot data to assess each tree detection algorithm/parameter set by converting the
 432 distance-from-center and azimuth measurements of the trees in the field plots to x-y positions relative to the
 433 field plot centers distinguishable in the Level 2 reflectance maps as the orange fabric X’s that we laid out
 434 prior to each flight. In the reflectance maps, we located 110 out of 160 field plot centers while some plot
 435 centers were obscured due to dense interlocking tree crowns or because a plot center was located directly
 436 under a single tree crown. For each of the 110 field plots with identifiable plot centers– the “validation field
 437 plots”, we calculated 7 forest structure metrics using the ground data collected by Fettig et al. ¹⁴: total
 438 number of trees, number of trees greater than 15 m in height, mean height of trees, 25th percentile tree height,
 439 75th percentile tree height, mean distance to nearest tree neighbor, and mean distance to second nearest
 440 neighbor. For each tree detection algorithm and parameter set described above, we calculated the same set of
 441 7 structure metrics within the footprint of the validation field plots. We calculated the Pearson’s correlation
 442 and root mean square error (RMSE) between the ground data and the aerial data for each of the 7 structure
 443 metrics for each of the 177 automatic tree detection algorithms/parameter sets. For each algorithm and
 444 parameter set, we calculated its performance relative to other algorithms as whether its Pearson’s correlation
 445 was within 5% of the highest Pearson’s correlation as well as whether its RMSE was within 5% of the lowest
 446 RMSE. We summed the number of forest structure metrics for which it reached these 5% thresholds for
 447 each algorithm/parameter set. For automatically detecting trees across the whole study, we selected the
 448 algorithm/parameter set that performed well across the most forest metrics (see Results).

449 We delineated individual tree crowns (Figure 4; Level 3a, fourth image; Supplementary Figure 15) with a
 450 marker controlled watershed segmentation algorithm⁹⁹ implemented in the `ForestTools` package⁹⁷ using the
 451 detected treetops as markers. If the automatic segmentation algorithm failed to generate a crown segment for
 452 a detected tree (e.g., often snags with a very small crown footprint), a circular crown was generated with a
 453 radius of 0.5 m. If the segmentation generated multiple polygons for a single detected tree, only the polygon
 454 containing the detected tree was retained. Because image overlap decreases near the edges of the overall flight
 455 path and reduces the quality of the SfM processing in those areas, we excluded segmented crowns within 35 m

456 of the edge of the survey area. Given the narrower field of view of the Rededge3 multispectral camera versus
457 the X3 RGB camera whose optical parameters were used to define the ~40 ha survey area around each site,
458 as well as the 35 m additional buffering, the survey area at each site was ~30 ha (see Supplementary Table 1).

459 **Level 3b: Data derived from spectral and geometric information** We overlaid the segmented
460 crowns on the reflectance maps from 20 sites spanning the latitudinal and elevation gradient in the study.
461 Using QGIS (<https://qgis.org/en/site/>), we hand classified 564 trees as live/dead and as one of 5 dominant
462 species in the study area (ponderosa pine, *Pinus lambertiana*, *Abies concolor*, *Calocedrus decurrens*, or
463 *Quercus kelloggii*) using the mapped ground data as a guide. Each tree was further classified as “host” for
464 ponderosa pine or “non-host” for all other species.¹⁸ We extracted all the pixel values within each segmented
465 crown polygon from the five, Level 2 orthorectified reflectance maps (one per narrow band on the Rededge3
466 camera) as well as from the five, Level 3a vegetation index maps using the `velox` package.¹⁰⁰ For each crown
467 polygon, we calculated the mean value of the extracted Level 2 and Level 3a pixels and used them as ten
468 independent variables in a five-fold cross validated boosted logistic regression model to predict whether the
469 hand classified trees were alive or dead. For just the living trees, we similarly used all 10 mean reflectance
470 values per crown polygon to predict tree species using a five-fold cross validated regularized discriminant
471 analysis. The boosted logistic regression and regularized discriminant analysis were implemented using the
472 `caret` package in R.¹⁰¹ We used these models to classify all tree crowns in the data set as alive or dead
473 (Figure 4; Level 3b, first image; Supplementary Figure 16) as well as to classify the species of living trees
474 (and then host or non-host; Figure 4; Level 3b, second image; Supplementary Figure 17).

475 Because the tops of dead, needle-less trees are narrow, they may not be well-represented in the point
476 clouds produced using SfM photogrammetry, which biases their height estimates downward. Further, field
477 measurements can overestimate the heights of live trees relative to aerial survey methods.¹⁰² To correct these
478 measurement biases, we calibrated aerial tree height measurements to ground-based height measurements.
479 Specifically, we identified the crowns of 451 field-measured trees in the drone-derived tree data, modeled the
480 relationship between field- and drone-measured tree heights for both live and dead trees, and used the models
481 to adjust the drone-measured tree heights (See Supplementary Methods). We applied a conservative height
482 correction to live and dead trees based on trees measured by the drone to be greater than 20 m in height that
483 increased dead tree height by an average of 2.8 m and reduced the heights of live trees by an average of 0.9
484 m (See Supplementary Figures 18-20 and Supplementary Note 2). Finally, we estimated the basal area of
485 each tree from their corrected drone-measured height using species-specific simple linear regressions of the
486 relationship between height and DBH as measured in the coincident field plots from Fettig et al.¹⁴.

487 We note that our study relies on the generation of Level 3a products in order to combine them and create Level
488 3b products like the classified tree maps, but this need not be the case. For instance, deep learning/neural
489 net methods may be able to use both the spectral and geometric information from lower level data products
490 simultaneously to locate and classify trees in a scene and directly generate Level 3b products without a need
491 to first generate the Level 3a products.^{103,104}

492 **Level 4: Aggregations to regular grids**

493 We rasterized the forest structure and composition data at a spatial resolution similar to that of the field
494 plots to better match the grain size at which we validated the automatic tree detection algorithms. In each
495 raster cell, we calculated: number of dead trees, number of ponderosa pine trees, total number of trees, and
496 mean height of ponderosa pine trees. The values of these variables in each grid cell and derivatives from them
497 were used for visualization and modeling. Here, we show the fraction of dead trees per cell (Figure 4; Level 4,
498 first image; Supplementary Figure 21), the fraction of host trees per cell (Figure 4; Level 4, second image),
499 the mean height of ponderosa pine trees in each cell (Figure 4; Level 4, third image), and the total count of
500 trees per cell (Figure 4; Level 4, fourth image).

501 **Note on assumptions about dead trees**

502 For the purposes of this study, we assumed that all dead trees were ponderosa pine and thus hosts colonized
503 by WPB. This is a reasonably good assumption for our study area; for example, Fettig et al.¹⁴ found that
504 73.4% of dead trees in their coincident field plots were ponderosa pine. Mortality was concentrated in the
505 larger-diameter classes and attributed primarily to WPB (see Figure 5 of Fettig et al.¹⁴). The species
506 contributing to the next highest proportion of dead trees was incense cedar which represented 18.72% of the
507 dead trees in the field plots. While the detected mortality is most likely to be ponderosa pine killed by WPB,
508 it is critical to interpret our results with these limitations in mind.

509 **Environmental data**

510 We used CWD¹⁰⁵ from the 1981-2010 mean value of the basin characterization model¹⁰⁶ as an integrated
511 measure of historic temperature and moisture conditions for each of the 32 sites. Higher values of CWD
512 correspond to historically hotter, drier conditions and lower values correspond to historically cooler, wetter
513 conditions. CWD has been shown to correlate well with broad patterns of tree mortality in the Sierra
514 Nevada¹¹ as well as bark beetle-induced tree mortality.¹⁰⁷ The forests along the entire CWD gradient used in
515 this study experienced exceptional hot drought between 2012 to 2016 with a severity of at least a 1,200-year
516 event, and perhaps more severe than a 10,000-year event.^{2,3} We converted the CWD value for each site into a

517 z-score representing that site’s deviation from the mean CWD across the climatic range of Sierra Nevada
518 ponderosa pine as determined from 179 herbarium records described in Baldwin et al.¹⁰⁸. Thus, a CWD
519 z-score of 1 would indicate that the CWD at that site is one standard deviation hotter/drier than the mean
520 CWD across all geolocated herbarium records for ponderosa pine in the Sierra Nevada.

521 **Statistical model**

522 We used a generalized linear model with a zero-inflated binomial response and a logit link to predict the
523 probability of ponderosa pine mortality within each 20 x 20-m cell using the total number of ponderosa
524 pine trees in each cell as the number of trials, and the number of dead trees in each cell as the number of
525 “successes”. As covariates, we used the proportion of trees that are WPB hosts (i.e., ponderosa pine) in each
526 cell, the mean height of ponderosa pine trees in each cell, the count of trees of all species (overall density) in
527 each cell, and the site-level CWD using Eq. 1. Note that the two-way interaction between the overall density
528 and the proportion of trees that are hosts is directly proportional to the number of ponderosa pine trees in
529 the cell. We centered and scaled all predictor values, and used weakly-regularizing default priors from the
530 `brms` package.¹⁰⁹ To measure and account for spatial autocorrelation underlying ponderosa pine mortality,
531 we subsampled the data at each site to a random selection of 200, 20 x 20-m cells representing approximately
532 27.5% of the surveyed area. Additionally with these subsampled data, we included a separate exact Gaussian
533 process term per site of the noncentered/nonscaled interaction between the x- and y-position of each cell
534 using the `gp()` function in the `brms` package.¹⁰⁹ The Gaussian process estimates the spatial covariance in the
535 response variable (log-odds of ponderosa pine mortality) jointly with the effects of the other covariates.

$$y_{i,j} \sim \begin{cases} 0, & p \\ \text{Binom}(n_i, \pi_i), & 1 - p \end{cases}$$

$$\begin{aligned} \text{logit}(\pi_i) = & \beta_0 + \\ & \beta_1 X_{cwd,j} + \beta_2 X_{propHost,i} + \beta_3 X_{PipoHeight,i} + \\ & \beta_4 X_{overallDensity,i} + \beta_5 X_{overallBA,i} + \\ & \beta_6 X_{cwd,j} X_{PipoHeight,i} + \beta_7 X_{cwd,j} X_{propHost,i} + \\ & \beta_8 X_{cwd,j} X_{overallDensity,i} + \beta_9 X_{cwd,j} X_{overallBA,i} + \\ & \beta_{10} X_{propHost,i} X_{PipoHeight,i} + \beta_{11} X_{propHost,i} X_{overallDensity,i} + \\ & \beta_{12} X_{PipoHeight,i} X_{overallBA,i} + \\ & \beta_{13} X_{cwd,j} X_{propHost,i} X_{PipoHeight,i} + \\ & \mathcal{GP}_j(x_i, y_i) \end{aligned} \tag{1}$$

536 Where y_i is the number of dead trees in cell i , n_i is the sum of the dead trees (assumed to be ponderosa pine)
537 and live ponderosa pine trees in cell i , π_i is the probability of ponderosa pine tree mortality in cell i , p is the
538 probability of there being zero dead trees in a cell arising as a result of an independent, unmodeled process,
539 $X_{cwd,j}$ is the z-score of CWD for site j , $X_{propHost,i}$ is the scaled proportion of trees that are ponderosa pine
540 in cell i , $X_{PipoHeight,i}$ is the scaled mean height of ponderosa pine trees in cell i , $X_{overallDensity,i}$ is the scaled
541 density of all trees in cell i , $X_{overallBA,i}$ is the scaled basal area of all trees in cell i , x_i and y_i are the x- and
542 y- coordinates of the centroid of the cell in an EPSG3310 coordinate reference system, and \mathcal{GP}_j represents
543 the exact Gaussian process describing the spatial covariance between cells at site j .

544 We fit this model using the `brms` package¹⁰⁹ which implements the No U-Turn Sampler extension to the
545 Hamiltonian Monte Carlo algorithm¹¹⁰ in the Stan programming language.¹¹¹ We used 4 chains with 5000
546 iterations each (2000 warmup, 3000 samples), and confirmed chain convergence by ensuring all `Rhat` values
547 were less than 1.1¹¹² and that the bulk and tail effective sample sizes (ESS) for each estimated parameter
548 were greater than 100 times the number of chains (i.e., greater than 400 in our case). We used posterior
549 predictive checks to visually confirm model performance by overlaying the density curves of the predicted
550 number of dead trees per cell over the observed number.¹¹³ For the posterior predictive checks, we used
551 50 random samples from the model fit to generate 50 density curves and ensured curves were centered on
552 the observed distribution, paying special attention to model performance at capturing counts of zero (see
553 Supplementary Figure 22).

554 **Data availability**

555 All field and drone data processed for this study are available via the Open Science Framework at <https://doi.org/10.17605/OSF.IO/3CWF9>.¹¹⁴ The administrative boundaries file for the USDA Forest Service
556 (S_USA.AdministrativeForest.shp) can be found at [https://data.fs.usda.gov/geodata/edw/datasets.ph](https://data.fs.usda.gov/geodata/edw/datasets.php?dsetCategory=boundaries)
557 [p?dsetCategory=boundaries](https://data.fs.usda.gov/geodata/edw/datasets.php?dsetCategory=boundaries). The 2014 version of the 1981-2010 thirty-year historic average climatic water
558 deficit data (cwd1981_2010_ave_HST_1550861123.tif) can be found on the California Climate Commons
559 at <http://climate.calcommons.org/dataset/2014-CA-BCM>. The dataset representing ponderosa pine
560 geolocations derived from herbaria records (California_Species_clean_All_epsg_3310.csv) can be found
561 at <https://doi.org/10.6078/D16K5W>.¹¹⁵ The vector file representing Jepson geographic subdivisions of
562 California and used to define the Sierra Nevada region can be requested at <https://ucjeps.berkeley.edu/eflora>
563 [/geography.html](https://ucjeps.berkeley.edu/eflora/geography.html).
564

565 **Code availability**

566 Statistical analyses were performed using the `brms` packages. With the exception of the SfM software
567 (Pix4Dmapper Cloud) and the GIS software QGIS, all data carpentry and analyses were performed using
568 R.¹¹⁶ All code used to generate the results from this study are available via GitHub at [https://github](https://github.com/mikoontz/local-structure-wpb-severity)
569 [ub.com/mikoontz/local-structure-wpb-severity](https://github.com/mikoontz/local-structure-wpb-severity) and is mirrored on the Open Science Framework at
570 <https://doi.org/10.17605/OSF.IO/WPK5Z>.¹¹⁷

571 **Acknowledgements**

572 We gratefully acknowledge funding from the USDA Forest Service Western Wildlands Environmental Threat
573 Assessment Center (WWETAC) and the Pacific Southwest Research Station Climate Change Competitive
574 Grant Program. We thank Connie Millar for comments and guidance during the development of this project,
575 and Meagan Oldfather for her role as visual observer during drone flights. We thank Beverly Bulaon for
576 her significant contribution to field plot network establishment. We also thank Victoria Scholl for helpful
577 discussions regarding remotely-sensed data product levels, and Derek Young for helpful discussions while
578 revising this manuscript. We gratefully acknowledge the Map Pilot for iOS team (who implemented several
579 feature requests that helped us conduct our drone flights), Pix4D (which provided free cloud infrastructure
580 for much of the Structure from Motion photogrammetry processing), and the Open Science Framework
581 (who facilitated the public access to our complete dataset). Thanks to Alex Mandel, Dan Krofcheck, Taylor
582 Nelson, Nate Metzler, Brandon Stark, Andy Wong, Grace Liu, Sean Hogan, the Micasense team, Lawrence
583 Dennis from Aerial Technology International, and Casey Neistat for valuable input regarding drones, sensors,

584 safe flying, and SfM photogrammetry. Publication of this article was partially funded by the University of
585 Colorado Boulder Libraries Open Access Fund and the University of California, Davis Library Open Access
586 Fund.

587 **Author contributions**

588 Author contributions are defined using the Contributor Roles Taxonomy (CRediT; <https://casrai.org/credit/>).
589 Conceptualization: MJK, AML, CJF, MPN, LAM; Data curation: MJK; Formal analysis: MJK; Funding
590 acquisition: MJK, MPN, CJF, AML; Investigation: MJK, LAM, CJF; Methodology: MJK, AML; Project
591 administration: MJK, MPN, AML; Resources: MJK, MPN, AML; Software: MJK; Supervision: MJK, MPN,
592 AML; Validation: MJK; Visualization: MJK; Writing – original draft: MJK; Writing – review and editing:
593 MJK, AML, CJF, MPN, LAM

594 **Competing interests**

595 The authors declare no competing interests.

References

- 596 1. USDAFS. Press Release: Survey finds 18 million trees died in California in 2018. [https://www.fs.usda.gov](https://www.fs.usda.gov/Internet/FSE_DOCUMENTS/FSEPRD609321.pdf)
597 v/Internet/FSE_DOCUMENTS/FSEPRD609321.pdf (2019).
- 598 2. Griffin, D. & Anchukaitis, K. J. How unusual is the 2012-2014 California drought? *Geophysical Research*
599 *Letters* **41**, 9017–9023 (2014).
- 600 3. Robeson, S. M. Revisiting the recent California drought as an extreme value. *Geophysical Research Letters*
601 **42**, 6771–6779 (2015).
- 602 4. Asner, G. P. *et al.* Progressive forest canopy water loss during the 2012-2015 California drought. *Proceedings*
603 *of the National Academy of Sciences* **113**, E249–E255 (2016).
- 604 5. Brodrick, P. G. & Asner, G. P. Remotely sensed predictors of conifer tree mortality during severe drought.
605 *Environ. Res. Lett.* **12**, 115013 (2017).
- 606 6. Fettig, C. J. Chapter 2: Forest health and bark beetles. in *Managing Sierra Nevada Forests. PSW-GTR-237*
607 (USDA Forest Service, 2012).
- 608 7. Kolb, T. E. *et al.* Observed and anticipated impacts of drought on forest insects and diseases in the United
609 States. *Forest Ecology and Management* **380**, 321–334 (2016).
- 610 8. Waring, R. H. & Pitman, G. B. Modifying lodgepole pine stands to change susceptibility to mountain pine
611 beetle attack. *Ecology* **66**, 889–897 (1985).
- 612 9. Restaino, C. *et al.* Forest structure and climate mediate drought-induced tree mortality in forests of the
613 Sierra Nevada, USA. *Ecological Applications* **0**, e01902 (2019).
- 614 10. USDAFS. Press Release: Record 129 million dead trees in California. [https://www.fs.usda.gov/Internet](https://www.fs.usda.gov/Internet/FSE_DOCUMENTS/fseprd566303.pdf)
615 /FSE_DOCUMENTS/fseprd566303.pdf (2017).
- 616 11. Young, D. J. N. *et al.* Long-term climate and competition explain forest mortality patterns under extreme
617 drought. *Ecology Letters* **20**, 78–86 (2017).
- 618 12. Raffa, K. F. *et al.* Cross-scale drivers of natural disturbances prone to anthropogenic amplification: The
619 dynamics of bark beetle eruptions. *BioScience* **58**, 501–517 (2008).
- 620 13. Boone, C. K., Aukema, B. H., Bohlmann, J., Carroll, A. L. & Raffa, K. F. Efficacy of tree defense
621 physiology varies with bark beetle population density: A basis for positive feedback in eruptive species. *Can.*
622 *J. For. Res.* **41**, 1174–1188 (2011).
- 623

- 624 14. Fettig, C. J., Mortenson, L. A., Bulaon, B. M. & Foulk, P. B. Tree mortality following drought in the
625 central and southern Sierra Nevada, California, U.S. *Forest Ecology and Management* **432**, 164–178 (2019).
- 626 15. Stephenson, N. L., Das, A. J., Ampersee, N. J. & Bulaon, B. M. Which trees die during drought? The
627 key role of insect host-tree selection. *Journal of Ecology* **75**, 2383–2401 (2019).
- 628 16. Senf, C., Campbell, E. M., Pflugmacher, D., Wulder, M. A. & Hostert, P. A multi-scale analysis of
629 western spruce budworm outbreak dynamics. *Landscape Ecol* **32**, 501–514 (2017).
- 630 17. Seidl, R. *et al.* Small beetle, large-scale drivers: How regional and landscape factors affect outbreaks of
631 the European spruce bark beetle. *J Appl Ecol* **53**, 530–540 (2016).
- 632 18. Fettig, C. J. Native bark beetles and wood borers in Mediterranean forests of California. in *Insects and*
633 *diseases of Mediterranean Forest systems* 499–528 (Springer International Publishing, 2016).
- 634 19. Raffa, K. F. & Berryman, A. A. The role of host plant resistance in the colonization behavior and ecology
635 of bark beetles (Coleoptera: Scolytidae). *Ecological Monographs* **53**, 27–49 (1983).
- 636 20. Logan, J. A., White, P., Bentz, B. J. & Powell, J. A. Model analysis of spatial patterns in mountain pine
637 beetle outbreaks. *Theoretical Population Biology* **53**, 236–255 (1998).
- 638 21. Wallin, K. F. & Raffa, K. F. Feedback between individual host selection behavior and population dynamics
639 in an eruptive herbivore. *Ecological Monographs* **74**, 101–116 (2004).
- 640 22. Franceschi, V. R., Krokene, P., Christiansen, E. & Krekling, T. Anatomical and chemical defenses of
641 conifer bark against bark beetles and other pests. *New Phytologist* **167**, 353–376 (2005).
- 642 23. Raffa, K. F., Grégoire, J.-C. & Staffan Lindgren, B. Natural history and ecology of bark beetles. in *Bark*
643 *Beetles* 1–40 (Elsevier, 2015). doi:10.1016/B978-0-12-417156-5.00001-0.
- 644 24. Bentz, B. J. *et al.* Climate change and bark beetles of the western United States and Canada: Direct and
645 indirect effects. *BioScience* **60**, 602–613 (2010).
- 646 25. DeRose, R. J. & Long, J. N. Drought-driven disturbance history characterizes a southern Rocky Mountain
647 subalpine forest. *Can. J. For. Res.* **42**, 1649–1660 (2012).
- 648 26. Hart, S. J., Veblen, T. T., Schneider, D. & Molotch, N. P. Summer and winter drought drive the initiation
649 and spread of spruce beetle outbreak. *Ecology* **98**, 2698–2707 (2017).
- 650 27. Netherer, S., Panassiti, B., Pennerstorfer, J. & Matthews, B. Acute drought Is an important driver of
651 bark beetle infestation in Austrian Norway spruce stands. *Front. For. Glob. Change* **2**, (2019).

- 652 28. Kaiser, K. E., McGlynn, B. L. & Emanuel, R. E. Ecohydrology of an outbreak: Mountain pine beetle
653 impacts trees in drier landscape positions first. *Ecohydrology* **6**, 444–454 (2013).
- 654 29. Marini, L. *et al.* Climate drivers of bark beetle outbreak dynamics in Norway spruce forests. *Ecography*
655 **40**, 1426–1435 (2017).
- 656 30. Sambaraju, K. R., Carroll, A. L. & Aukema, B. H. Multiyear weather anomalies associated with range
657 shifts by the mountain pine beetle preceding large epidemics. *Forest Ecology and Management* **438**, 86–95
658 (2019).
- 659 31. Hayes, C. J., Fettig, C. J. & Merrill, L. D. Evaluation of multiple funnel traps and stand characteristics
660 for estimating western pine beetle-caused tree mortality. *Journal of Economic Entomology* **102**, 2170–2182
661 (2009).
- 662 32. Thistle, H. W. *et al.* Surrogate pheromone plumes in three forest trunk spaces: Composite statistics and
663 case studies. *Forest Science* **50**, (2004).
- 664 33. Miller, J. M. & Keen, F. P. *Biology and control of the western pine beetle: A summary of the first fifty*
665 *years of research.* (US Department of Agriculture, 1960).
- 666 34. Chubaty, A. M., Roitberg, B. D. & Li, C. A dynamic host selection model for mountain pine beetle,
667 *Dendroctonus ponderosae* Hopkins. *Ecological Modelling* **220**, 1241–1250 (2009).
- 668 35. Graf, M., Reid, M. L., Aukema, B. H. & Lindgren, B. S. Association of tree diameter with body size and
669 lipid content of mountain pine beetles. *The Canadian Entomologist* **144**, 467–477 (2012).
- 670 36. Geiszler, D. R. & Gara, R. I. Mountain pine beetle attack dynamics in lodgepole pine. in *Theory and*
671 *Practice of Mountain Pine Beetle Management in Lodgepole Pine Forests: Symposium Proceedings.* A. A.
672 *Berryman, G. D. Amman and R. W. Stark (Eds)* (1978).
- 673 37. Klein, W. H., Parker, D. L. & Jensen, C. E. Attack, emergence, and stand depletion trends of the
674 mountain pine beetle in a lodgepole pine stand during an outbreak. *Environ Entomol* **7**, 732–737 (1978).
- 675 38. Mitchell, R. G. & Preisler, H. K. Analysis of spatial patterns of lodgepole pine attacked by outbreak
676 populations of the mountain pine beetle. *Forest Science* **37**, 1390–1408 (1991).
- 677 39. Preisler, H. K. Modelling spatial patterns of trees attacked by bark-beetles. *Applied Statistics* **42**, 501
678 (1993).
- 679 40. Jactel, H. & Brockerhoff, E. G. Tree diversity reduces herbivory by forest insects. *Ecology Letters* **10**,
680 835–848 (2007).

- 681 41. Faccoli, M. & Bernardinelli, I. Composition and elevation of spruce forests affect susceptibility to bark
682 beetle attacks: Implications for forest management. *Forests* **5**, 88–102 (2014).
- 683 42. Berryman, A. A. Population dynamics of bark beetles. in *Bark Beetles in North American Conifers: A*
684 *System for the Study of Evolutionary Biology* 264–314 (1982).
- 685 43. Fettig, C. J. *et al.* The effectiveness of vegetation management practices for prevention and control of
686 bark beetle infestations in coniferous forests of the western and southern United States. *Forest Ecology and*
687 *Management* **238**, 24–53 (2007).
- 688 44. Moeck, H. A., Wood, D. L. & Lindahl, K. Q. Host selection behavior of bark beetles (Coleoptera:
689 Scolytidae) attacking *Pinus ponderosa*, with special emphasis on the western pine beetle, *Dendroctonus*
690 *brevicomis*. *Journal of Chemical Ecology* **7**, 49–83 (1981).
- 691 45. Evenden, M. L., Whitehouse, C. M. & Sykes, J. Factors influencing flight capacity of the mountain pine
692 beetle (Coleoptera: Curculionidae: Scolytinae). *Environ Entomol* **43**, 187–196 (2014).
- 693 46. Raffa, K. F. & Berryman, A. A. Accumulation of monoterpenes and associated volatiles following
694 inoculation of grand fir with a fungus transmitted by the fir engraver, *Scolytus ventralis* (Coleoptera:
695 Scolytidae). *The Canadian Entomologist* **114**, 797–810 (1982).
- 696 47. Anderegg, W. R. L. *et al.* Tree mortality from drought, insects, and their interactions in a changing
697 climate. *New Phytologist* **208**, 674–683 (2015).
- 698 48. Kane, V. R. *et al.* Assessing fire effects on forest spatial structure using a fusion of Landsat and airborne
699 LiDAR data in Yosemite National Park. *Remote Sensing of Environment* **151**, 89–101 (2014).
- 700 49. Larson, A. J. & Churchill, D. Tree spatial patterns in fire-frequent forests of western North America,
701 including mechanisms of pattern formation and implications for designing fuel reduction and restoration
702 treatments. *Forest Ecology and Management* **267**, 74–92 (2012).
- 703 50. Morris, J. L. *et al.* Managing bark beetle impacts on ecosystems and society: Priority questions to
704 motivate future research. *Journal of Applied Ecology* **54**, 750–760 (2017).
- 705 51. Shiklomanov, A. N. *et al.* Enhancing global change experiments through integration of remote-sensing
706 techniques. *Frontiers in Ecology and the Environment* **0**, (2019).
- 707 52. Jeronimo, S. M. A. *et al.* Forest structure and pattern vary by climate and landform across active-fire
708 landscapes in the montane Sierra Nevada. *Forest Ecology and Management* **437**, 70–86 (2019).
- 709 53. Roussel, J.-R., Auty, D., De Boissieu, F. & Meador, A. S. *lidR: Airborne LiDAR data manipulation and*

- 710 *visualization for forestry applications*. (2019).
- 711 54. McDowell, N. *et al.* Mechanisms of plant survival and mortality during drought: Why do some plants
712 survive while others succumb to drought? *New Phytologist* **178**, 719–739 (2008).
- 713 55. Seybold, S. J. *et al.* Management of western North American bark beetles with semiochemicals. *Annual*
714 *Review of Entomology* **63**, 407–432 (2018).
- 715 56. Fettig, C. J., McKelvey, S. R. & Huber, D. P. W. Nonhost angiosperm volatiles and Verbenone disrupt
716 response of western pine beetle, *Dendroctonus brevicomis* (Coleoptera: Scolytidae), to attractant-baited traps.
717 *ecen* **98**, 2041–2048 (2005).
- 718 57. Fettig, C. J., Dabney, C. P., McKelvey, S. R. & Huber, D. P. W. Nonhost angiosperm volatiles and
719 verbenone protect individual ponderosa pines from attack by western pine beetle and red turpentine beetle
720 (Coleoptera: Curculionidae, Scolytinae). *west j appl for* **23**, 40–45 (2008).
- 721 58. Fettig, C. J. *et al.* Efficacy of ‘Verbenone Plus’ for protecting ponderosa pine trees and stands from
722 *Dendroctonus brevicomis* (Coleoptera: Curculionidae) attack in British Columbia and California. *J Econ*
723 *Entomol* **105**, 1668–1680 (2012).
- 724 59. Oliver, W. W. Is self-thinning in ponderosa pine ruled by *Dendroctonus* bark beetles? in *Forest health*
725 *through silviculture: Proceedings of the 1995 National Silviculture Workshop* 6 (1995).
- 726 60. Fettig, C. & McKelvey, S. Resiliency of an interior ponderosa pine forest to bark beetle infestations
727 following fuel-reduction and forest-restoration treatments. *Forests* **5**, 153–176 (2014).
- 728 61. Fettig, C. J. & Hilszczański, J. Management strategies for bark beetles in conifer forests. in *Bark Beetles*
729 555–584 (Elsevier, 2015). doi:10.1016/B978-0-12-417156-5.00014-9.
- 730 62. Chesson, P. Mechanisms of maintenance of species diversity. *Annual Review of Ecology and Systematics*
731 **31**, 343–366 (2000).
- 732 63. Fricker, G. A. *et al.* More than climate? Predictors of tree canopy height vary with scale in complex
733 terrain, Sierra Nevada, CA (USA). *Forest Ecology and Management* **434**, 142–153 (2019).
- 734 64. Ma, S., Concilio, A., Oakley, B., North, M. & Chen, J. Spatial variability in microclimate in a mixed-conifer
735 forest before and after thinning and burning treatments. *Forest Ecology and Management* **259**, 904–915
736 (2010).
- 737 65. Stovall, A. E. L., Shugart, H. & Yang, X. Tree height explains mortality risk during an intense drought.
738 *Nature Communications* **10**, 1–6 (2019).

- 739 66. Stephenson, N. L. & Das, A. J. Height-related changes in forest composition explain increasing tree
740 mortality with height during an extreme drought. *Nature Communications* **11**, 3402 (2020).
- 741 67. Stovall, A. E. L., Shugart, H. H. & Yang, X. Reply to ‘Height-related changes in forest composition
742 explain increasing tree mortality with height during an extreme drought’. *Nature Communications* **11**, 3401
743 (2020).
- 744 68. Person, H. L. Tree selection by the western pine beetle. *J for* **26**, 564–578 (1928).
- 745 69. Person, H. L. Theory in explanation of the selection of certain trees by the western pine beetle. *J for* **29**,
746 696–699 (1931).
- 747 70. Pile, L. S., Meyer, M. D., Rojas, R., Roe, O. & Smith, M. T. Drought impacts and compounding mortality
748 on forest trees in the southern Sierra Nevada. *Forests* **10**, 237 (2019).
- 749 71. Frey, J., Kovach, K., Stemmler, S. & Koch, B. UAV photogrammetry of forests as a vulnerable process.
750 A sensitivity analysis for a structure from motion RGB-image pipeline. *Remote Sensing* **10**, 912 (2018).
- 751 72. James, M. R. & Robson, S. Mitigating systematic error in topographic models derived from UAV and
752 ground-based image networks. *Earth Surface Processes and Landforms* **39**, 1413–1420 (2014).
- 753 73. Gray, P. C. *et al.* A convolutional neural network for detecting sea turtles in drone imagery. *Methods in*
754 *Ecology and Evolution* **10**, 345–355 (2019).
- 755 74. Millar, C. I., Stephenson, N. L. & Stephens, S. L. Climate change and forests of the future: Managing in
756 the face of uncertainty. *Ecological Applications* **17**, 2145–2151 (2007).
- 757 75. Vose, J. M. *et al.* Forests. In *Impacts, Risks, and Adaptation in the United States: The Fourth National*
758 *Climate Assessment, Volume II [Reidmiller, D. R., C. W. Avery, D. R. Easterling, K. E. Kunkel, K. L. M.*
759 *Lewis, T. K. Maycock, and B. C. Stewart (eds.)]*. 232–267 <https://nca2018.globalchange.gov/chapter/6/>
760 (2018) doi:10.7930/NCA4.2018.CH6.
- 761 76. Bedard, W. D. *et al.* Western pine beetle: Field response to its sex pheromone and a synergistic host
762 terpene, myrcene. *Science* **164**, 1284–1285 (1969).
- 763 77. Byers, J. A. & Wood, D. L. Interspecific inhibition of the response of the bark beetles, *Dendroctonus*
764 *brevicomis* and *Ips paraconfusus*, to their pheromones in the field. *J Chem Ecol* **6**, 149–164 (1980).
- 765 78. Shepherd, W. P., Huber, D. P. W., Seybold, S. J. & Fettig, C. J. Antennal responses of the western pine
766 beetle, *Dendroctonus brevicomis* (Coleoptera: Curculionidae), to stem volatiles of its primary host, *Pinus*
767 *ponderosa*, and nine sympatric nonhost angiosperms and conifers. *Chemoecology* **17**, 209–221 (2007).

- 768 79. DJI. Zenmuse X3 - Creativity Unleashed. <https://www.dji.com/zenmuse-x3/info> (2015).
- 769 80. Micasense. MicaSense. [https://support.micasense.com/hc/en-us/articles/215261448-RedEdge-User-](https://support.micasense.com/hc/en-us/articles/215261448-RedEdge-User-Manual-PDF-Download-)
770 [Manual-PDF-Download-](https://support.micasense.com/hc/en-us/articles/215261448-RedEdge-User-Manual-PDF-Download-) (2015).
- 771 81. DJI. DJI - The World Leader in Camera Drones/Quadcopters for Aerial Photography. [https://www.dji.](https://www.dji.com/matrice100/info)
772 [com/matrice100/info](https://www.dji.com/matrice100/info) (2015).
- 773 82. Wyngaard, J. *et al.* Emergent challenges for science sUAS data management: Fairness through community
774 engagement and best practices development. *Remote Sensing* **11**, 1797 (2019).
- 775 83. Rouse, W., Haas, R. H., Deering, W. & Schell, J. A. *Monitoring the vernal advancement and retrogradation*
776 *(green wave effect) of natural vegetation.* (1973).
- 777 84. DronesMadeEasy. Map Pilot for DJI on iOS. [https://itunes.apple.com/us/app/map-pilot-for-](https://itunes.apple.com/us/app/map-pilot-for-dji/id1014765000?mt=8)
778 [dji/id1014765000?mt=8](https://itunes.apple.com/us/app/map-pilot-for-dji/id1014765000?mt=8) (2018).
- 779 85. Farr, T. G. *et al.* The shuttle radar topography mission. *Reviews of Geophysics* **45**, (2007).
- 780 86. Zhang, W. *et al.* An easy-to-use airborne LiDAR data filtering method based on cloth simulation. *Remote*
781 *Sensing* **8**, 501 (2016).
- 782 87. Hijmans, R. J. *et al.* *Raster: Geographic data analysis and modeling.* (2019).
- 783 88. Gitelson, A. & Merzlyak, M. N. Spectral reflectance changes associated with autumn senescence of
784 *Aesculus hippocastanum* L. And *Acer platanoides* L. Leaves. Spectral features and relation to chlorophyll
785 estimation. *Journal of Plant Physiology* **143**, 286–292 (1994).
- 786 89. Coops, N. C., Johnson, M., Wulder, M. A. & White, J. C. Assessment of QuickBird high spatial resolution
787 imagery to detect red attack damage due to mountain pine beetle infestation. *Remote Sensing of Environment*
788 **103**, 67–80 (2006).
- 789 90. Clevers, J. G. P. W. & Gitelson, A. A. Remote estimation of crop and grass chlorophyll and nitrogen
790 content using red-edge bands on Sentinel-2 and -3. *International Journal of Applied Earth Observation and*
791 *Geoinformation* **23**, 344–351 (2013).
- 792 91. Li, W., Guo, Q., Jakubowski, M. K. & Kelly, M. A new method for segmenting individual trees from the
793 LiDAR point cloud. *Photogrammetric Engineering & Remote Sensing* **78**, 75–84 (2012).
- 794 92. Jakubowski, M. K., Li, W., Guo, Q. & Kelly, M. Delineating individual trees from LiDAR data: A
795 comparison of vector- and raster-based segmentation approaches. *Remote Sensing* **5**, 4163–4186 (2013).

- 796 93. Shin, P., Sankey, T., Moore, M. & Thode, A. Evaluating unmanned aerial vehicle images for estimating
797 forest canopy fuels in a ponderosa pine stand. *Remote Sensing* **10**, 1266 (2018).
- 798 94. Roussel, J.-R. *lidRplugins: Extra functions and algorithms for lidR package.* (2019).
- 799 95. Eysn, L. *et al.* A benchmark of LiDAR-based single tree detection methods using heterogeneous forest
800 data from the alpine space. *Forests* **6**, 1721–1747 (2015).
- 801 96. Vega, C. *et al.* PTrees: A point-based approach to forest tree extraction from LiDAR data. *International*
802 *Journal of Applied Earth Observation and Geoinformation* **33**, 98–108 (2014).
- 803 97. Plowright, A. *ForestTools: Analyzing remotely sensed forest data.* (2018).
- 804 98. Pau, G., Fuchs, F., Sklyar, O., Boutros, M. & Huber, W. EBImage: An R package for image processing
805 with applications to cellular phenotypes. *Bioinformatics* **26**, 979–981 (2010).
- 806 99. Meyer, F. & Beucher, S. Morphological segmentation. *Journal of Visual Communication and Image*
807 *Representation* **1**, 21–46 (1990).
- 808 100. Hunziker, P. *Velox: Fast raster manipulation and extraction.* (2017).
- 809 101. Kuhn, M. Building predictive models in R using the caret package. *Journal of Statistical Software* **28**,
810 1–26 (2008).
- 811 102. Wang, Y. *et al.* Is field-measured tree height as reliable as believed a comparison study of tree height
812 estimates from field measurement, airborne laser scanning and terrestrial laser scanning in a boreal forest.
813 *ISPRS Journal of Photogrammetry and Remote Sensing* **147**, 132–145 (2019).
- 814 103. Weinstein, B. G., Marconi, S., Bohlman, S., Zare, A. & White, E. Individual tree-crown detection in
815 RGB imagery using semi-supervised deep learning neural networks. *Remote Sensing* **11**, 1309 (2019).
- 816 104. dos Santos, A. A. *et al.* Assessment of CNN-Based Methods for Individual Tree Detection on Images
817 Captured by RGB Cameras Attached to UAVs. *Sensors (Basel)* **19**, (2019).
- 818 105. Stephenson, N. Actual evapotranspiration and deficit: Biologically meaningful correlates of vegetation
819 distribution across spatial scales. *Journal of Biogeography* **25**, 855–870 (1998).
- 820 106. Flint, L. E., Flint, A. L., Thorne, J. H. & Boynton, R. Fine-scale hydrologic modeling for regional
821 landscape applications: The California Basin Characterization Model development and performance. *Ecological*
822 *Processes* **2**, 25 (2013).
- 823 107. Millar, C. I. *et al.* Forest mortality in high-elevation whitebark pine (*Pinus albicaulis*) forests of eastern

- 824 California, USA: Influence of environmental context, bark beetles, climatic water deficit, and warming.
825 *Canadian Journal of Forest Research* **42**, 749–765 (2012).
- 826 108. Baldwin, B. G. *et al.* Species richness and endemism in the native flora of California. *American Journal*
827 *of Botany* **104**, 487–501 (2017).
- 828 109. Bürkner, P.-C. **brms**: An *R* package for bayesian multilevel models using Stan. *Journal of Statistical*
829 *Software* **80**, 1–28 (2017).
- 830 110. Hoffman, M. D. & Gelman, A. The No-U-Turn Sampler: Adaptively setting path lengths in Hamiltonian
831 Monte Carlo. *Journal of Machine Learning Research* **15**, 31 (2014).
- 832 111. Carpenter, B. *et al.* Stan: A Probabilistic Programming Language. *Journal of Statistical Software* **76**,
833 1–32 (2017).
- 834 112. Brooks, S. P. & Gelman, A. General methods for monitoring convergence of iterative simulations.
835 *Journal of Computational and Graphical Statistics* **7**, 434 (1998).
- 836 113. Gabry, J., Simpson, D., Vehtari, A., Betancourt, M. & Gelman, A. Visualization in Bayesian workflow.
837 *Journal of the Royal Statistical Society: Series A (Statistics in Society)* **182**, 389–402 (2019).
- 838 114. Koontz, M. J., Latimer, A. M., Mortenson, L. A., Fettig, C. J. & North, M. P. Drone-derived data
839 supporting "Cross-scale interaction of host tree size and climatic water deficit governs bark beetle-induced
840 tree mortality". (2020) doi:10.17605/OSF.IO/3CWF9.
- 841 115. Baldwin, B. G. *et al.* Master spatial file for native California vascular plants used by Baldwin *et al.*
842 (2017 Amer. J. Bot.). *Dryad* 3 (2017) doi:10.6078/D16K5W.
- 843 116. R Core Team. *R: A language and environment for statistical computing*. (R Foundation for Statistical
844 Computing, 2018).
- 845 117. Koontz, M. J., Latimer, A. M., Mortenson, L. A., Fettig, C. J. & North, M. P. Local-structure-wpb-
846 severity. (2019) doi:10.17605/OSF.IO/WPK5Z.